Hydrodynamic correlations in shear flow: Multiparticle-collision-dynamics simulation study

Anoop Varghese, Chien-Cheng Huang, Roland G. Winkler, and Gerhard Gompper
Institute of Complex Systems and Institute for Advanced Simulation, Forschungszentrum Jülich, Jülich 52425, Germany
(Received 26 August 2015; published 2 November 2015)

The nonequilibrium hydrodynamic correlations of a multiparticle-collision-dynamics (MPC) fluid in shear flow are studied by analytical calculations and simulations. The Navier-Stokes equations for a MPC fluid are linearized about the shear flow and the hydrodynamic modes are evaluated as an expansion in the wave vector. The shear-rate dependence and anisotropy of the transverse and longitudinal velocity correlations are analyzed. We demonstrate that hydrodynamic correlations in shear flow are anisotropic, specifically, the two transverse modes are no longer identical. In addition, our simulations reveal the directional dependence of the frequency and attenuation of the longitudinal velocity correlation function. Furthermore, the velocity autocorrelation functions of a tagged fluid particle in shear flow are determined. The simulation results for various hydrodynamic correlations agree very well with the theoretical predictions.

DOI: 10.1103/PhysRevE.92.053002 PACS number(s): 47.15.−x, 83.50.Ax, 47.11.−j, 05.20.Jj

I. INTRODUCTION

The thermodynamics of systems far from equilibrium has drawn growing interest in the past couple of decades [1]. Several nonequilibrium relations, collectively called fluctuation relations, have been derived for transient and steady nonequilibrium states. These relations have been verified using exactly solvable models and numerical simulations (see Ref. [1] and references therein). An interesting class of nonequilibrium systems is fluids under external fields such as shear flow and/or a temperature gradient [2]. Considerable progress has been achieved in understanding these systems using hydrodynamics calculations [3–8], numerical simulations [9–11], and experiments [12]. For instance, the fluctuation relation for entropy production has been verified in numerical simulations of simple fluids under shear flow [11,13]. Apart from satisfying fluctuation relations, nonequilibrium fluids show several interesting features that are absent in equilibrium. In particular, nonequilibrium hydrodynamic correlations in steady states are long-ranged even for fluids far from critical points [3,4,7,9,14]. In addition, these correlations are anisotropic, in contrast to equilibrium correlations in simple fluids. A consequence of the long-range nature of the correlations is the nonintensivity of pressure fluctuations [5].

Computer simulations are extremely valuable to study nonequilibrium phenomena. In particular, recently developed mesoscale hydrodynamic simulation approaches, such as lattice Boltzmann [15–17], dissipative particle dynamics (DPD) [18–20], or multiparticle collision dynamics (MPC) [21–23], permit us to cover large length and long time scales, and a wide range of external parameters such as shear rates and temperature gradients. All these approaches are essentially alternative ways of solving the Navier-Stokes equations for the fluid dynamics. Common to them is a simplified, coarse-grained description of the fluid degrees of freedom while maintaining the essential microscopic physics on the length scales of interest [23]. By now, the MPC method has successfully been applied in a broad range of equilibrium and nonequilibrium simulations of soft matter systems (see, e.g., Ref. [24] and references therein). In particular, the hydrodynamic correlations of the MPC fluid have been determined and it has been shown that they agree with the solutions of the fluctuating Landau-Lifshitz Navier-Stokes equations [25]. Moreover, the hydrodynamic correlations of embedded colloids [26–31] and polymers [32] have been calculated. Even more, MPC simulations have been successfully applied to verify the fluctuation relation for entropy production in shear flows [11]. So far, however, an analysis of nonequilibrium correlation functions of a MPC fluid and a comparison with theoretical approaches is missing.

In this paper, we fill this gap and determine analytically and by MPC simulations the time-correlation functions of hydrodynamic variables of a simple isothermal fluid under shear flow. We first derive analytical expressions for the respective correlations by linearizing the Navier-Stokes equations. To this end, we follow the methods employed in Refs. [3,8], where adiabatic or granular fluids are considered. Here, the isothermal approach is simpler, because energy is no longer a conserved quantity. We restrict ourselves to moderate shear rates for which the equal-time coupling between hydrodynamic modes can be ignored [3,10]. Exploiting the MPC method, we then perform shear flow simulations and calculate the respective hydrodynamic correlation functions. The primary effect of shear is the anisotropy of the hydrodynamic correlation functions, as already predicted in Refs. [3,10]. The frequency and attenuation of the longitudinal modes become directional and shear rate dependent. In addition, the degeneracy of the two transverse modes, present at equilibrium, is removed. The anisotropy of the longitudinal and transverse velocity autocorrelations is also manifested in the anisotropy of the velocity autocorrelations of tagged MPCs particles. Moreover, the correlation functions show a faster decay than the equilibrium correlations at long times. By comparison, we find excellent agreement between the theoretical predictions and the MPC simulation results.

The article is organized as follows. The theoretical expressions for the velocity correlation functions are derived in Sec. II. Section III presents simulation results and a comparison with the theoretical predictions. Our results and findings are summarized in Sec. IV. More details of the calculations are presented in the Appendices.

II. THEORY

A. Linearized Navier-Stokes equations under shear

The Navier-Stokes equations of an isothermal MPC fluid are given by

$$\frac{\partial \rho}{\partial t} = -\nabla \cdot (\rho \mathbf{u}), \tag{1}$$

$$\rho\left[\frac{\partial}{\partial t} + \mathbf{u}\cdot\nabla\right]\mathbf{u} = -\nabla p + \eta\nabla^2\mathbf{u} + \frac{\eta^k}{3}\nabla(\nabla\cdot\mathbf{u}). \tag{2}$$

They account for mass and momentum conservation, where $\rho(\mathbf{x},\mathbf{t})$ is the mass density, $\mathbf{u}(\mathbf{x},\mathbf{t})$ the fluid velocity field, and $p(\mathbf{x},\mathbf{t})$ the pressure field at the position $\mathbf{x}$ at time t. The shear viscosity is denoted as η. The Navier-Stokes equations are adopted to a non-angular-momentum-conserving MPC fluid, hence, the kinetic contribution η^k of the shear viscosity appears in the last term in the right-hand side of Eq. (2), rather than the viscosity η itself [25,33]. The equations are then linearized by setting $\rho = \rho_0 + \delta\rho$, $p = p_0 + \delta p$, and $\mathbf{u} = \mathbf{u}_0 + \delta\mathbf{u}$, where $u_{0\alpha} = \gamma_{\alpha\beta}x_\beta$, with the shear-rate tensor $\gamma_{\alpha\beta}$ and $\alpha,\beta \in \{x,y,z\}$. We choose the x and y axis of the Cartesian coordinate system as the flow and the gradient direction, respectively, such that $\gamma_{\alpha\beta} = \dot\gamma\delta_{\alpha x}\delta_{\beta y}$, where $\dot\gamma$ is the shear rate. We use the summation convention for Greek indices unless otherwise stated. Equations (1) and (2) can then be written as

$$\left[\frac{\partial}{\partial t} + \gamma_{\alpha\beta}x_\beta\frac{\partial}{\partial x_\alpha}\right]\delta\rho = -\rho_0\nabla\cdot\delta\mathbf{u}, \tag{3}$$

$$\rho_0\left[\frac{\partial}{\partial t} + \gamma_{\alpha'\beta}x_\beta\frac{\partial}{\partial x_{\alpha'}}\right]\delta u_\alpha = -\rho_0\gamma_{\alpha\beta}\delta u_\beta - \frac{\partial}{\partial x_\alpha}\delta p + \eta\nabla^2\delta u_\alpha + \frac{\eta^k}{3}\frac{\partial}{\partial x_\alpha}(\nabla\cdot\delta\mathbf{u}). \tag{4}$$

Here, we have neglected second-order terms in the fluctuations. We eliminate δp with the ideal gas equation of state, $\delta p = c_T^2\delta\rho$, where c_T is the isothermal velocity of sound. By rescaling the velocity and density according to $\delta\mathbf{u} \equiv \delta\mathbf{u}/c_T$ and $\delta\rho \equiv \delta\rho/\rho_0$, Eqs. (3) and (4) can be written in momentum space as

$$\left[\frac{\partial}{\partial t} - \gamma_{\alpha\beta}k_\alpha\frac{\partial}{\partial k_\beta}\right]\delta\tilde\rho = ic_T\mathbf{k}\cdot\delta\tilde{\mathbf{u}}, \tag{5}$$

$$\left[\frac{\partial}{\partial t} - \gamma_{\alpha'\beta}k_{\alpha'}\frac{\partial}{\partial k_\beta}\right]\delta\tilde u_\alpha = -\gamma_{\alpha\beta}\delta\tilde u_\beta + ic_Tk_\alpha\delta\tilde\rho - \nu k^2\delta\tilde u_\alpha - \frac{\nu^k}{3}k_\alpha k_\beta\delta\tilde u_\beta, \tag{6}$$

with the kinematic viscosities $\nu = \eta/\rho_0$, $\nu^k = \eta^k/\rho_0$. The variables with a tilde are Fourier-transformed variables according to the definition

$$\tilde{\mathbf{f}}(\mathbf{k}) = \int d^3\mathbf{x}\, e^{i\mathbf{k}\cdot\mathbf{x}}\,\mathbf{f}(\mathbf{x}). \tag{7}$$

We now write the above equations in terms of the longitudinal and transverse components of the velocity field. Let $\delta\tilde{\mathbf{u}} = \delta\tilde u^{(1)}\mathbf{e}^{(1)} + \delta\tilde u^{(2)}\mathbf{e}^{(2)} + \delta\tilde u^{(3)}\mathbf{e}^{(3)}$, where $\mathbf{e}^{(1)}$, $\mathbf{e}^{(2)}$, and $\mathbf{e}^{(3)}$ are three orthogonal unit vectors. Here, $\mathbf{e}^{(1)}$ is chosen along the direction of $\hat{\mathbf{k}}$, so that $\delta\tilde u^{(1)}$ is the longitudinal, and $\delta\tilde u^{(2)}$ and $\delta\tilde u^{(3)}$ are the transverse components of the velocity field. By introducing the vector $\tilde{\mathbf{z}} = (\delta\tilde\rho,\delta\tilde u^{(1)},\delta\tilde u^{(2)},\delta\tilde u^{(3)})^T$, the Navier-Stokes equations can be written as

$$\left[\frac{\partial}{\partial t} - \dot\gamma k_x\frac{\partial}{\partial k_y}\right]\tilde{\mathbf{z}} + \mathcal{L}\tilde{\mathbf{z}} = 0. \tag{8}$$

The explicit form of the matrix $\mathcal{L}$ for the choice [3]

$$\mathbf{e}^{(1)} = \mathbf{k}/|\mathbf{k}|, \tag{9}$$

$$\mathbf{e}^{(2)} = \left[\hat{\mathbf{y}} - e_y^{(1)}\mathbf{e}^{(1)}\right]/\hat k_\perp, \tag{10}$$

$$\mathbf{e}^{(3)} = \mathbf{e}^{(1)}\times\mathbf{e}^{(2)} \tag{11}$$

of the unit vectors is given in Appendix A. Here, $\hat{\mathbf{y}}$ is the unit vector along the y axis in the Cartesian coordinate system and $\hat k_\perp = (k_x^2 + k_z^2)^{1/2}/k$, where $k = |\mathbf{k}|$. The solution to the above equation can be written as the linear combination

$$\tilde{\mathbf{z}}(\mathbf{k},t) = \sum_{i=1}^{4} a^{(i)}(\mathbf{k},t)\boldsymbol{\xi}^{(i)}(\mathbf{k}) \tag{12}$$

of the eigenvectors $\boldsymbol{\xi}^{(i)}(\mathbf{k})$, which satisfy the eigenvalue equation

$$\left[-\dot\gamma k_x\frac{\partial}{\partial k_y} + \mathcal{L}\right]\boldsymbol{\xi}^{(i)}(\mathbf{k}) = \lambda_i\boldsymbol{\xi}^{(i)}(\mathbf{k}). \tag{13}$$

Let $\boldsymbol{\eta}^{(i)}(\mathbf{k})$ be the corresponding left eigenvectors such that

$$\sum_{l=1}^{4}\eta_l^{(i)}\xi_l^{(j)} = \delta_{ij}. \tag{14}$$

The left and right eigenvectors and the eigenvalues can be calculated using perturbation theory [3] and are given in Appendix B. Inserting $\tilde{\mathbf{z}}(\mathbf{k},t)$ from Eq. (12) into Eq. (8) and using Eq. (13) together with the orthogonality condition in Eq. (14), we obtain

$$\left[\frac{\partial}{\partial t} - \dot\gamma k_x\frac{\partial}{\partial k_y} + \lambda_i(\mathbf{k})\right]a^{(i)}(\mathbf{k},t) = 0. \tag{15}$$

The solution of this equation can be expressed as [8]

$$a^{(i)}(\mathbf{k},t) = a^{(i)}(\mathbf{k}(-t),0)\exp\left[-\int_0^t d\tau\,\lambda_i(\mathbf{k}(-\tau))\right], \tag{16}$$

with the time-dependent $\mathbf{k}$ vector, $\mathbf{k}(t) = (k_x, k_y - \dot\gamma t k_x, k_z)^T$. Using Eqs. (12) and (16) and the relation $a^{(i)}(\mathbf{k},0) = \sum_{l=1}^4\eta_l^{(i)}(\mathbf{k})\tilde z_l(\mathbf{k},0)$, we get

$$\tilde z_i(\mathbf{k},t) = \sum_{j=1}^{4} G_{ij}(\mathbf{k},t)\tilde z_j(\mathbf{k}(-t),0), \tag{17}$$

where the propagator $G_{ij}(\mathbf{k},t)$ is defined as

$$G_{ij}(\mathbf{k},t) = \sum_{l=1}^{4}\xi_i^{(l)}(\mathbf{k})\eta_j^{(l)}(\mathbf{k}(-t))\exp\left[-\int_0^t d\tau\,\lambda_l(\mathbf{k}(-\tau))\right]. \tag{18}$$

In order to compare with simulation results, it is convenient to rewrite Eq. (17) by setting $\mathbf{k} = \mathbf{k}(t)$, i.e., by replacing k_y by $k_y - \dot\gamma t k_x$. We then get

$$\tilde z_i(\mathbf{k}(t),t) = \sum_{j=1}^{4} G_{ij}(\mathbf{k}(t),t)\tilde z_j(\mathbf{k},0), \tag{19}$$

with

$$G_{ij}(\mathbf{k}(t),t) = \sum_{l=1}^{4} \xi_i^{(l)}(\mathbf{k}(t))\eta_j^{(l)}(\mathbf{k}) \exp\left[-\int_0^t d\tau \lambda_l(\mathbf{k}(\tau))\right], \tag{20}$$

using $[\int_0^t d\tau \lambda_i(\mathbf{k}(-\tau))]_{\mathbf{k}=\mathbf{k}(t)} = \int_0^t d\tau \lambda_i(\mathbf{k}(\tau))$. The explicit form of $G_{ij}(\mathbf{k}(t),t)$ can be obtained from the eigenvectors $\{\boldsymbol{\xi},\boldsymbol{\eta}\}$ and the eigenvalues λ_l given in Appendix B. Note that the solution given by Eq. (19) represents the evolution of the hydrodynamic variables in the time-dependent reference frame in the $\mathbf{k}$ space.

B. Hydrodynamic correlation functions

The correlations of the hydrodynamic variables are defined as $C_{ij}(\mathbf{k},\mathbf{k}',t) = \langle \tilde z_i(\mathbf{k}(t),t)\tilde z_j(\mathbf{k}',0)\rangle$, and become with Eq. (19)

$$C_{ij}(\mathbf{k},\mathbf{k}',t) = \sum_{l=1}^{4} G_{il}(\mathbf{k}(t),t)\langle \tilde z_l(\mathbf{k},0)\tilde z_j(\mathbf{k}',0)\rangle. \tag{21}$$

The correlations $\langle \tilde z_i(\mathbf{k},0)\tilde z_j(-\mathbf{k},0)\rangle$ vanishes at equilibrium, i.e., $\dot\gamma = 0$, for $i \neq j$. However, they are, in general, nonzero for $\dot\gamma \neq 0$. We consider only small shear rates $\dot\gamma \lesssim \nu k^2$, for which these cross-correlations can be neglected, as discussed in Refs. [3,10]. Hence, the correlation functions can be written as $C_{ij}(\mathbf{k},\mathbf{k}',t) \simeq (2\pi)^3\delta_{ij}\delta(\mathbf{k}+\mathbf{k}')C_{ii}(\mathbf{k},t)$, where $C_{ii}(\mathbf{k},t) = \langle \tilde z_i(\mathbf{k},0)\tilde z_i(-\mathbf{k},0)\rangle G_{ii}(\mathbf{k}(t),t)$. Using the explicit expressions for the propagators $G_{ii}(\mathbf{k}(t),t)$, the correlation functions can be written as

$$C_{11}(\mathbf{k},t) = \frac{\rho_0 k_B T}{c_T^2}\left(\frac{k(t)}{k}\right)^{1/2} e^{-\frac{1}{2}\tilde\nu\chi(\mathbf{k},t)}\cos[c_T\phi(\mathbf{k},t)], \tag{22}$$

$$C_{22}(\mathbf{k},t) = \frac{c_T^2}{\rho_0^2}C_{11}(\mathbf{k},t), \tag{23}$$

$$C_{33}(\mathbf{k},t) = \frac{k_B T}{\rho_0}\left(\frac{k}{k(t)}\right)e^{-\nu\chi(\mathbf{k},t)}, \tag{24}$$

$$C_{44}(\mathbf{k},t) = \frac{k_B T}{\rho_0}e^{-\nu\chi(\mathbf{k},t)}, \tag{25}$$

where $\phi(\mathbf{k},t)$ and $\chi(\mathbf{k},t)$ are given by

$$\phi(\mathbf{k},t) = \frac{1}{2\dot\gamma k_x}\left[[k_y k - k_y(t)k(t)] - k_\perp^2 \ln\left(\frac{k_y(t)+k(t)}{k_y+k}\right)\right], \tag{26}$$

$$\chi(\mathbf{k},t) = k^2 t - \dot\gamma k_x k_y t^2 + \frac{1}{3}\dot\gamma^2 k_x^2 t^3, \tag{27}$$

and $k(t) = |\mathbf{k}(t)|$. Here, $\tilde\nu = \nu + \nu^k/3$, and the equilibrium relations $\langle \tilde z_1(\mathbf{k},0)\tilde z_1(-\mathbf{k},0)\rangle = \rho_0 k_B T c_T^{-2}$ and $\langle \tilde z_i(\mathbf{k},0)\tilde z_i(-\mathbf{k},0)\rangle = \rho_0^{-1}k_B T$ for $i = 2,3,4$ have been employed. These expressions can be derived using fluctuating hydrodynamics for a MPC fluid [25]; however, we do not present the derivations here.

A few remarks on the correlation functions given by Eqs. (22)–(25) are in order. In the limit $\dot\gamma \to 0$, we get $\phi(\mathbf{k},t) \to kt$ and $\chi(\mathbf{k},t) \to k^2 t$, and therefore the correlation functions are reduced to the corresponding equilibrium relations [25,34] to $\mathcal{O}(k^2)$. In the absence of shear, the correlation functions for an isothermal MPC fluid can be obtained for all orders in k; the explicit expressions for the velocity autocorrelation functions are provided in Ref. [25]. We also note that the expression for $C_{33}(\mathbf{k},t)$ remains exact for all shear rates within the order we are working at, even if the neglected equal-time correlations of the form $\langle \tilde z_i(\mathbf{k},0)\tilde z_j(-\mathbf{k},0)\rangle$ for $i \neq j$ are taken into account. By the same token, $C_{44}(\mathbf{k},t)$ is exact for all shear rates for $k_z = 0$.

C. Velocity correlations in real space

From Eq. (17), the velocity correlation function follows as

$$\langle \delta\tilde{\mathbf{u}}(\mathbf{k},t)\cdot\delta\tilde{\mathbf{u}}(\mathbf{k}',0)\rangle = (2\pi)^3\delta(\mathbf{k}(-t)+\mathbf{k}')C^u(\mathbf{k},t), \tag{28}$$

with the abbreviation

$$C^u(\mathbf{k},t) = \sum_{i=2}^{4} C_{ii}(\mathbf{k}(-t),t)\mathbf{e}^{(i-1)}(\mathbf{k})\cdot\mathbf{e}^{(i-1)}(\mathbf{k}(-t)) \tag{29}$$

and by using $C_{ij}(\mathbf{k},t) \simeq 0$ for $i \neq j$. The velocity autocorrelation in real space is then given by

$$\langle \delta\mathbf{u}(\mathbf{x},t)\cdot\delta\mathbf{u}(\mathbf{0},0)\rangle = \frac{1}{(2\pi)^3}\int d^3\mathbf{k}C^u(\mathbf{k},t)e^{-i\mathbf{k}\cdot\mathbf{x}}. \tag{30}$$

The velocity autocorrelation function $C(t) = \langle \mathbf{v}(t)\cdot\mathbf{v}(0)\rangle$ of a tagged particle of velocity $\mathbf{v}(t)$ can be obtained by setting $\mathbf{v}(t) = \mathbf{u}(\mathbf{r},t)$, where $\mathbf{r}$ is the position of the tagged particle, and averaging over all its positions $\mathbf{r}$. Hence, we obtain

$$C(t) = \frac{1}{(2\pi)^3}\int d^3\mathbf{k}C^u(\mathbf{k},t)\langle e^{-i\mathbf{k}\cdot\mathbf{r}}\rangle, \tag{31}$$

with the definition $\langle e^{i\mathbf{k}\cdot\mathbf{r}}\rangle = \int d^3\mathbf{r}P(\mathbf{r},t)e^{-i\mathbf{k}\cdot\mathbf{r}}$, and $P(\mathbf{r},t)$ the distribution function of the position of the tagged particle. Using the Fourier representation of $P(\mathbf{r},t)$, we get $\langle e^{-i\mathbf{k}\cdot\mathbf{r}}\rangle = P(\mathbf{k},t)$. In shear flow, $P(\mathbf{k},t)$ follows from the advective diffusion equation [35]

$$\left[\frac{\partial}{\partial t} - \dot\gamma k_x\frac{\partial}{\partial k_y}\right]P(\mathbf{k},t) = -Dk^2P(\mathbf{k},t), \tag{32}$$

where D is the diffusion coefficient. The solution of the equation can be expressed as

$$P(\mathbf{k},t) = P(\mathbf{k}(-t),0)\exp\left[-D\int_0^t d\tau k^2(-\tau)\right]. \tag{33}$$

Then, Eq. (31) yields

$$C(t) = \frac{1}{(2\pi)^3}\int d^3\mathbf{k}\, C^u(\mathbf{k},t)P(\mathbf{k}(-t),0) \tag{34}$$

$$\times\exp\left[-D\int_0^t d\tau k^2(-\tau)\right]. \tag{35}$$

By changing the integration variable from $\mathbf{k}$ to $\mathbf{k}(t)$, and using the fact that the Jacobian of the transformation is unity, we get

$$C(t) = \frac{1}{(2\pi)^3} \int d^3\mathbf{k}\, C^u(\mathbf{k}(t),t) \exp\left[-D \int_0^t d\tau k^2(\tau)\right] \tag{36}$$

by using $P(\mathbf{k},0) = 1$ [36].

So far, we considered infinitely large systems. In computer simulations, however, finite-size systems are used with typically periodic boundary conditions. This leads to a discrete set $\mathbf{k_n}$ of wave vectors, with $k_{\alpha,n} = 2\pi n_\alpha / L$, where L is the length of the cubic simulation box of volume $V = L^3$, $n_\alpha \in \mathbb{Z}$, and $\mathbf{k_n} \neq 0$. Hence, the correlation function becomes

$$C(t) = \frac{1}{V} \sum_{\mathbf{k_n}=-\infty}^{\infty} C^u(\mathbf{k_n}(t),t) \exp\left[-D \int_0^t d\tau \mathbf{k_n}^2(\tau)\right]. \tag{37}$$

The velocity autocorrelation function in shear flow is anisotropic. Therefore, we write the above equation in terms of the components corresponding to the three orthogonal directions as

$$C_\alpha(t) = \frac{1}{V} \sum_{\mathbf{k_n}=-\infty}^{\infty} \sum_{l=1}^{3} C_{jj}(\mathbf{k_n},t) e_\alpha^{(l)}(\mathbf{k_n}) e_\alpha^{(l)}(\mathbf{k_n}(t)), \tag{38}$$

where $j = l + 1$. Note that index α is not summed over. Since MPC is a particle-based mesoscale simulation method, the validity of the Navier-Stokes equation breaks down at the level of a collision cell [25]. Therefore, the k values in the summation in Eq. (38) are limited by a cutoff corresponding to the smallest hydrodynamic length scale. Alternative but similar approaches to evaluate the velocity autocorrelations of a tagged fluid particle can be found in Refs. [8,10].

III. SIMULATIONS

A. Multiparticle collision dynamics

In the MPC approach, the fluid is represented by point-particles [22,23]. Their time evolution proceeds in two independent steps, namely streaming and collision. In the streaming step, the particles move ballistically, i.e., the particle positions are updated as

$$\mathbf{x}_i(t+h) = \mathbf{x}_i(t) + h\mathbf{v}_i(t), \tag{39}$$

where h is the collision-time step. Here, $\mathbf{x}_i$ denotes the position of particle i, $\mathbf{v}_i$ its velocity, and $i \in \{1,\ldots,N\}$, with the total number of particles N. In the collision step, the particles are grouped into cubic cells of length a, and a rotation of their relative velocities—with respect to the center-of-mass velocity of the particular cell—is performed. Hence, the new velocities are

$$\mathbf{v}_i(t+h) = \mathbf{V}_{\rm cm}(t) + \mathcal{R}(\alpha)[\mathbf{v}_i(t) - \mathbf{V}_{\rm cm}(t)]. \tag{40}$$

Here, $V_{\rm cm}(t)$ is the center-of-mass velocity of the cell that contains the particle i and $\mathcal{R}(\alpha)$ is the rotation matrix, with the axis of rotation taken as a random unit vector. A random shift of the collision cell lattice is performed at every collision step to ensure Galilean invariance [23,37].

We perform isothermal simulations, where temperature is maintained by the cell-level Maxwell-Boltzmann-scaling (MBS) approach, which has been shown to yield a canonical ensemble [24,38]. The hydrodynamic fluctuations of the MPC fluid supplemented by the MBS method is known to be consistent with the linearized Navier-Stokes equation in equilibrium [24,25]. Shear flow is implemented by Lees-Edwards boundary conditions [39–41]. The time step of our simulations is chosen as $h/\tau = 0.1$, with the unit of time $\tau = \sqrt{ma^2/k_BT}$, to ensure a large Schmidt number [42], and the average number of particles in a collision cell is set to 10. The numerical values of the transport coefficients for this choice of the simulation parameters are $\nu = 0.870a^2/\tau$, $\tilde{\nu} = 0.887a^2/\tau$, $D = 0.051a^2/\tau$, $c_T = 1.0a/\tau$ [23].

B. Hydrodynamic correlations

The density and velocity fields in $\mathbf{k}$ space are defined as

$$\tilde{\rho}(\mathbf{k},t) = \sum_{i=1}^{N} e^{i\mathbf{k}(t)\cdot\mathbf{x}_i}, \tag{41}$$

$$\delta\tilde{\mathbf{u}}(\mathbf{k},t) = \sum_{i=1}^{N} [\mathbf{v}_i - \mathbf{u}_0(\mathbf{x}_i)] e^{i\mathbf{k}(t)\cdot\mathbf{x}_i}, \tag{42}$$

where $\mathbf{u}_0(\mathbf{x}) = \dot{\gamma} y \hat{\mathbf{x}}$ is the mean velocity field. Note that we use the time-dependent $\mathbf{k}$ vector $\mathbf{k}(t) = (k_x, k_y - \dot{\gamma} t k_x, k_z)$, so that the allowed $\mathbf{k}$ vectors are consistent with the Lees-Edwards boundary conditions. The direction as well as the magnitude of this $\mathbf{k}$ vector change in time. The transverse and longitudinal components of the velocity field are then defined as $\delta u^{(i)}(\mathbf{k}(t),t) = \mathbf{e}^{(i)}(\mathbf{k}(t)) \cdot \delta\tilde{\mathbf{u}}(\mathbf{k},t)$. Here, the mutually orthogonal unit vectors $\mathbf{e}^{(i)}$ are given by Eqs. (9)–(11). For $k_x \neq 0$ and $\dot{\gamma} \neq 0$, the vectors $\mathbf{e}^{(1)}$ and $\mathbf{e}^{(2)}$ change direction with time in the plane normal to $\mathbf{e}^{(3)}$, which itself is constant in time.

A few notes on the calculation of autocorrelation functions in shear flow implemented via the Lees-Edwards boundary condition are in order. In equilibrium simulations, the origin of time is arbitrary, and therefore the moving-time-origin scheme [40] for calculating time correlation functions can be employed to improve statistics and to avoid storing position and velocity coordinates of the particles. However, in our simulations, the $\mathbf{k}$ vector is taken as a function of time and the time origin is taken as the time at which the image of a particle in the infinite periodic system is given by $\mathbf{x}_i' = \mathbf{x}_i + \mathbf{L}$, where $\mathbf{x}_i$ is the position of the particle in the primary simulation box and $\mathbf{L} = L(n_x, n_y, n_z)^T$. Therefore, averages have to be taken only over the allowed time origins. In addition, in order to be consistent with the definition of the time-dependent $\mathbf{k}$ vector, the position coordinate in the gradient direction has to be taken in the range $[-L_y/2, L_y/2]$. However, the usual moving-time-origin scheme can be employed in the evaluation of real-space time-correlation functions.

1. Correlation functions in momentum space

Figure 1 shows the numerically evaluated transverse velocity correlation function given by Eq. (25). As is evident from the theoretical expression, there are primarily two time regimes for the decay of the correlations. For $t \ll 1/\dot{\gamma}$, the

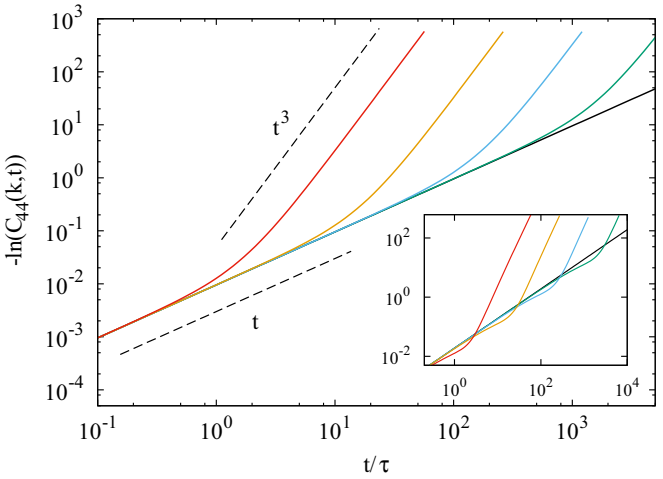

FIG. 1. (Color online) Theoretical predictions of the transverse velocity correlation function along $\mathbf{e}^{(3)}(\mathbf{k})$ [see Eqs. (11) and (25)]. The lines (solid) correspond to the shear rates $\dot{\gamma}\tau = 0.0, 0.001, 0.01, 0.1, 1.0$ (right to left). In the main figure, the wave vector components are $k_x = 2\pi/60$ and $k_y = k_z = 0$, and in the inset $k_x = k_y = 2\pi/60$ and $k_z = 0$.

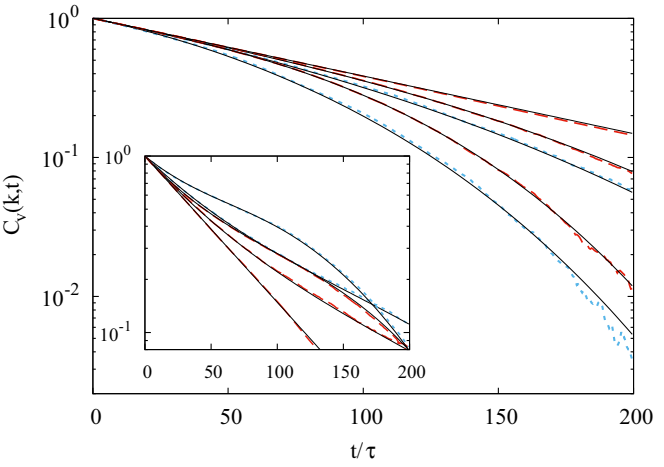

FIG. 2. (Color online) Theoretical and simulation results for the transverse velocity correlation functions along $\mathbf{e}^{(2)}(\mathbf{k})$ (blue, dotted) and $\mathbf{e}^{(3)}(\mathbf{k})$ (red, dashed) for the shear rates $\dot{\gamma}\tau = 0.0, 0.005, 0.01$ (top to bottom for the main figure and bottom to top for the inset at $t/\tau = 100$). The two transverse components are identical for $\dot{\gamma}\tau = 0.0$, and therefore only one of them (red, dashed) is presented. The solid lines (black) represent the theoretical results. In the main figure, the wave-vector components are $k_x = 2\pi/L$ and $k_y = k_z = 0$, and in the inset $k_x = k_y = 2\pi/L$ and $k_z = 0$.

decay is dominated by the term linear in t in the exponential [see Eq. (27)] and therefore is identical to the decay of the correlation function in equilibrium. However, for $t \gg 1/\dot{\gamma}$, the decay is dominated by the term proportional to t^3 and is characteristic of the shear flow. This term originates from the advection term in the Navier-Stokes equation and results in several interesting features such as a faster decaying long-time tail, with a power-law $t^{-5/2}$, of the velocity autocorrelation function of a tagged fluid particle [10], and a renormalization of the viscosity [43].

In Fig. 2 we compare the transverse velocity correlations obtained from the simulations and the theoretical expressions. In contrast to equilibrium correlations, the velocity autocorrelations of the two transverse components in shear flow are not identical. The transverse velocity component ($\mathbf{e}^{(3)}$ direction) perpendicular to the gradient direction decays slower than the second component ($\mathbf{e}^{(2)}$ direction) perpendicular to the longitudinal direction for long times ($t \gg 1/\dot{\gamma}$). Even though the distinction between the two transverse components is apparent from our simulations, it may be ignored in deriving the long-time tail exponents for the velocity autocorrelation function of a tagged fluid particle [10,43]. The transverse correlations, as mentioned in the previous paragraph, decay similar to those in equilibrium for $t \ll 1/\dot{\gamma}$ and faster for $t \gg 1/\dot{\gamma}$. For $t \approx 1/\dot{\gamma}$, the decay depends on the direction of the $\mathbf{k}$ vector, i.e., on the relative sign of k_x and k_y. For $\mathrm{sgn}(k_x) = \mathrm{sgn}(k_y)$, both transverse correlations decay slower than the equilibrium correlations, and faster otherwise (see insets of Figs. 1 and 2). For $k_y = 0$, the transverse correlation functions decay faster than the equilibrium correlations at all times.

The longitudinal velocity correlation function corresponds to sound propagation in the fluid. There are two effects of shear flow on the propagation of sound in an isothermal fluid—the modification of the sound damping factor and the change in the sound frequency and velocity (Doppler effect), both of which depend on the shear rate and the direction of propagation. Figure 3 shows the variation of longitudinal velocity correlations in the flow direction ($k_y = k_z = 0$) for different shear rates. The change in the frequency and the faster attenuation with increasing shear rate is well demonstrated. Figure 4 displays the anisotropy of the sound propagation. The frequency decreases when the sound propagation is in the direction along the flow and increases in the direction against the flow. The direction dependence of the attenuation of longitudinal velocity correlations is the same as that of the transverse velocity correlations. The autocorrelation function

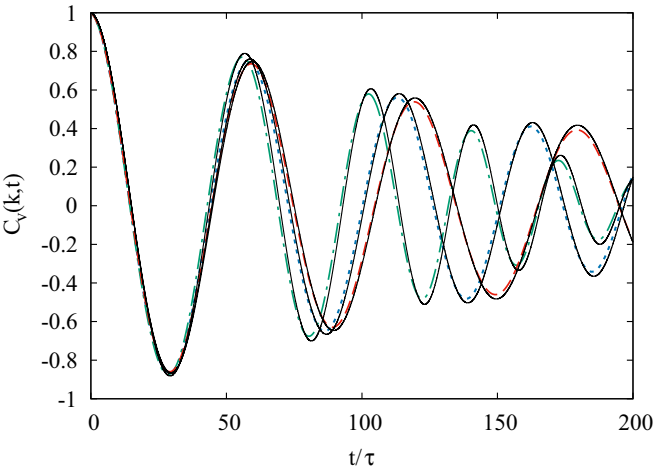

FIG. 3. (Color online) Longitudinal velocity correlations for the shear rates $\dot{\gamma}\tau = 0.0$ (red, dashed) 0.005 (blue, dotted), and 0.01 (green, dotted-dashed). The solid lines (black) represent theoretical results. The wave-vector components are $k_x = 2\pi/L$ and $k_y = k_z = 0$.

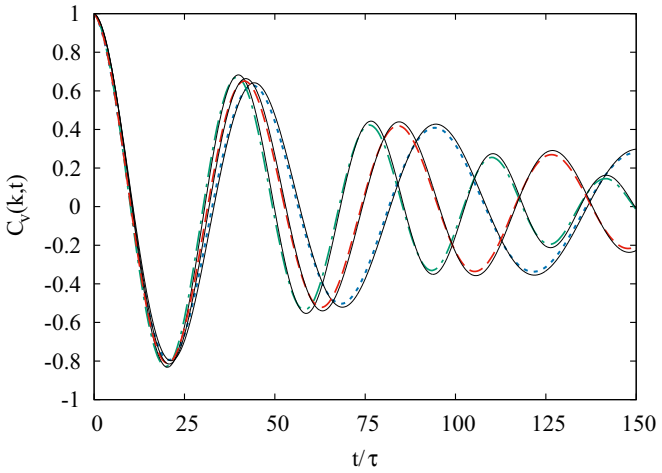

FIG. 4. (Color online) Longitudinal velocity correlations for $\dot{\gamma}\tau = 0.0$, $k_x = k_y = 2\pi/L$ (red, dashed), $\dot{\gamma}\tau = 0.005$, $k_x = k_y = 2\pi/L$ (blue, dotted), and $\dot{\gamma}\tau = 0.005$, $k_x = -k_y = 2\pi/L$ (green, dotted-dashed) . $k_z = 0$ for all the curves. The solid (back) lines represent the theoretical results.

of the density fluctuations shows an identical behavior as the longitudinal velocity correlations, and therefore we do present the results here.

2. Long-time behavior of velocity correlations

Figure 5 shows velocity autocorrelation functions of a tagged particle. Note that we consider the thermal velocity of the particle, i.e., the velocity with respect to the mean flow velocity. Evidently, the correlations in the three orthogonal directions are not identical. We find excellent agreement between theory and simulation results for long times. The deviations at short times are caused on the one hand by the fact that the theoretical hydrodynamic correlations are only accurate to $\mathcal{O}(k^2)$. On the other hand, partition of the MPC fluid in collision cells leads to a breakdown of hydrodynamics at short times and length scales below the collision-cell size [25]. However, the long-time behavior is determined by small **k** values, i.e., large length scales, which are correctly reproduced in the simulations.

IV. SUMMARY AND CONCLUSIONS

We have studied the nonequilibrium hydrodynamic time correlations of an isothermal MPC fluid under shear flow. We find good agreement between simulation results and theoretical predictions based on the linearized Navier-Stokes equations for moderate shear rates. We confirm that hydrodynamic correlations in shear flow are anisotropic, in agreement with previous studies [3,8,9]. Specifically, and in contrast to equilibrium correlations, the time correlations of the two transverse modes in Fourier space are no longer identical. In addition, our simulations reveal the directional dependence of the frequency and attenuation of the longitudinal velocity correlation function. As a consequence, the velocity autocorrelation function of a tracer fluid particle (MPC particle) is also anisotropic. The agreement between analytical calculations and simulations confirms that MPC is a suitable approach to study hydrodynamic properties of simple fluids under nonequilibrium conditions.

Our studies are restricted to moderate shear rates, where equal-time correlations of the hydrodynamic variables can be approximated by the corresponding equilibrium values. For high shear rates, this approximation does not hold and we observe significant deviations of the simulation results from the theoretical expressions. In order to theoretically evaluate the equal-time and autocorrelation functions for high shear rates, the fluctuating part of the stress tensor has to be explicitly included in the Navier-Stokes equations [3], which we took into account only implicitly. In addition, it is also necessary to take into account the density dependence of the viscosity in linearizing the Navier-Stokes equation. These issues will be addressed in future publications.

ACKNOWLEDGMENTS

Financial support of the project by the EU through FP7-Infrastructure ESMI (Grant No. 262348) is gratefully acknowledged.

APPENDIX A: THE HYDRODYNAMIC MATRIX

The evolution of the hydrodynamic variables are given by

$$\left[\frac{\partial}{\partial t} - \dot{\gamma} k_x \frac{\partial}{\partial k_y}\right]\tilde{\mathbf{z}} + \mathcal{L}\tilde{\mathbf{z}} = 0, \tag{A1}$$

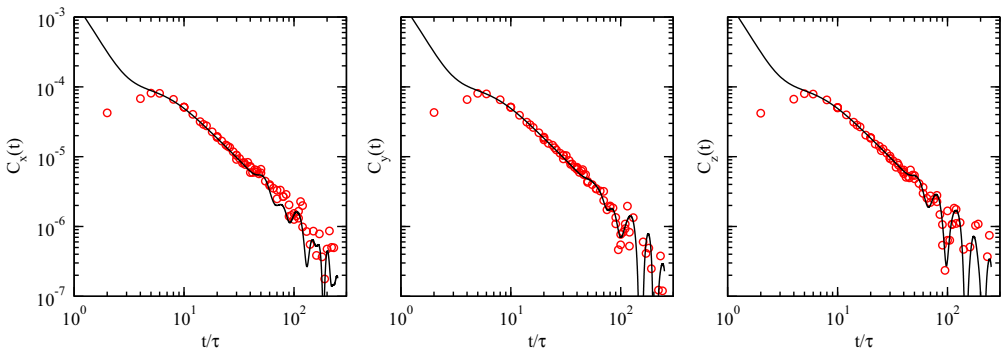

FIG. 5. (Color online) Velocity autocorrelation functions of a tagged particle along the various spatial directions. The shear rate is $\dot{\gamma}\tau = 0.01$. Simulation results are represented by open circles and the theoretical prediction by solid lines.

where $\mathcal{L} = -ik\mathcal{L}_1 + k^2\mathcal{L}_2 + \dot{\gamma}\mathcal{L}_3$, with

$$\mathcal{L}_1 = \begin{pmatrix} 0 & c_T & 0 & 0 \\ c_T & 0 & 0 & 0 \\ 0 & 0 & 0 & 0 \\ 0 & 0 & 0 & 0 \end{pmatrix},$$

$$\mathcal{L}_2 = \begin{pmatrix} 0 & 0 & 0 & 0 \\ 0 & \tilde{\nu} & 0 & 0 \\ 0 & 0 & \nu & 0 \\ 0 & 0 & 0 & \nu \end{pmatrix}, \tag{A2}$$

$$\mathcal{L}_3 = \begin{pmatrix} 0 & 0 & 0 & 0 \\ 0 & \Gamma_{11} & \Gamma_{12} & \Gamma_{13} \\ 0 & \Gamma_{21} & \Gamma_{22} & \Gamma_{23} \\ 0 & \Gamma_{31} & \Gamma_{32} & \Gamma_{33} \end{pmatrix},$$

$\tilde{\nu} = \nu + \nu^k/3$, and the matrix $\mathbf{\Gamma}$

$$\dot{\gamma}\Gamma_{ij} = e_m^{(i)}\gamma_{ml}e_l^{(j)} - e_n^{(i)}\gamma_{ml}k_m\frac{\partial}{\partial k_l}e_n^{(j)}. \tag{A3}$$

For the particular choice of the unit vectors $\mathbf{e}^{(i)}$ as given in Eqs. (9)–(11), the matrix $\mathbf{\Gamma}$ takes the form

$$\mathbf{\Gamma} = \begin{pmatrix} k_xk_y/k^2 & 2k_xk_\perp/k^2 & 0 \\ -k_x/k_\perp & -k_xk_y/k^2 & 0 \\ -k_yk_z/kk_\perp & -k_z/k & 0 \end{pmatrix}, \tag{A4}$$

where $k_\perp^2 = k_x^2 + k_z^2$.

APPENDIX B: EIGENVALUES AND EIGENVECTORS

The eigenvalue equation, Eq. (13), can be solved perturbatively by expanding $\boldsymbol{\xi}^{(m)}$ and λ_m in powers of k:

$$\begin{aligned} \boldsymbol{\xi}^{(m)} &= \boldsymbol{\xi}_0^{(m)} + k\boldsymbol{\xi}_1^{(m)} + \dots \\ \lambda_m &= k\lambda_{m,0} + k^2\lambda_{m,1} + \dots \end{aligned} \tag{B1}$$

The solution to the order $\mathcal{O}(k^2)$ is given by

$$\begin{aligned} \lambda_1 &= -ic_Tk + \frac{1}{2}(\tilde{\nu}k^2 + \dot{\gamma}k_xk_y/k^2), \\ \lambda_2 &= +ic_Tk + \frac{1}{2}(\tilde{\nu}k^2 + \dot{\gamma}k_xk_y/k^2), \\ \lambda_3 &= \nu k^2 - \dot{\gamma}k_xk_y/k^2,\ \lambda_4 = \nu k^2, \\ \boldsymbol{\xi}^{(1)} &= \frac{1}{\sqrt{2}}(1,1,0,0)^T,\ \boldsymbol{\xi}^{(2)} = \frac{1}{\sqrt{2}}(1,-1,0,0)^T, \\ \boldsymbol{\xi}^{(3)} &= (0,0,1,M)^T,\ \boldsymbol{\xi}^{(4)} = (0,0,0,1)^T, \end{aligned} \tag{B2}$$

where

$$M(\mathbf{k}) = -\frac{kk_z}{k_xk_\perp}\arctan\left(\frac{k_y}{k_\perp}\right). \tag{B3}$$

The left eigenvectors $\boldsymbol{\eta}^{(i)}$, which satisfy the condition $\sum_{l=1}^4 \eta_l^{(i)}\xi_l^{(j)} = \delta_{ij}$, are given by

$$\boldsymbol{\eta}^{(m)} = \boldsymbol{\xi}^{(m)^T},\ \text{for } m = 1, 2, \tag{B4}$$

and

$$\boldsymbol{\eta}^{(3)} = (0, 0, 1, 0),\ \boldsymbol{\eta}^{(4)} = (0, 0, -M, 1). \tag{B5}$$

[1] U. Seifert, Rep. Prog. Phys **75**, 126001 (2012).
[2] J. M. O. De Zarate and J. V. Sengers, *Hydrodynamic Fluctuations in Fluids and Fluid Mixtures* (Elsevier, New York, 2006).
[3] J. Lutsko and J. W. Dufty, Phys. Rev. A **32**, 3040 (1985).
[4] J. Machta, I. Oppenheim, and I. Procaccia, Phys. Rev. A **22**, 2809 (1980).
[5] H. Wada and S.-I. Sasa, Phys. Rev. E **67**, 065302 (2003).
[6] J. M. O. de Zárate and J. V. Sengers, J. Stat. Phys. **115**, 1341 (2004).
[7] J. M. Ortiz de Zárate and J. V. Sengers, Phys. Rev. E **77**, 026306 (2008).
[8] M. Otsuki and H. Hayakawa, Eur. Phys. J. Special Topics **179**, 179 (2009).
[9] M. Otsuki and H. Hayakawa, Phys. Rev. E **79**, 021502 (2009).
[10] M. Otsuki and H. Hayakawa, J. Stat. Mech. (2009) L08003.
[11] M. Belushkin, R. Livi, and G. Foffi, Phys. Rev. Lett. **106**, 210601 (2011).
[12] P. N. Segrè, R. W. Gammon, J. V. Sengers, and B. M. Law, Phys. Rev. A **45**, 714 (1992).
[13] D. J. Evans, E. G. D. Cohen, and G. P. Morriss, Phys. Rev. Lett. **71**, 2401 (1993).
[14] J. F. Lutsko and J. W. Dufty, Phys. Rev. E **66**, 041206 (2002).
[15] G. R. McNamara and G. Zanetti, Phys. Rev. Lett. **61**, 2332 (1988).
[16] X. Shan and H. Chen, Phys. Rev. E **47**, 1815 (1993).
[17] X. He and L.-S. Luo, Phys. Rev. E **56**, 6811 (1997).
[18] P. J. Hoogerbrugge and J. M. V. A. Koelman, Europhys. Lett. **19**, 155 (1992).
[19] P. Español and P. B. Warren, Europhys. Lett. **30**, 191 (1995).
[20] P. Español, Phys. Rev. E **52**, 1734 (1995).
[21] A. Malevanets and R. Kapral, J. Chem. Phys. **110**, 8605 (1999).
[22] R. Kapral, Adv. Chem. Phys. **140**, 89 (2008).
[23] G. Gompper, T. Ihle, D. M. Kroll, and R. G. Winkler, Adv. Polym. Sci. **221**, 1 (2009).
[24] C.-C. Huang, A. Varghese, G. Gompper, and R. G. Winkler, Phys. Rev. E **91**, 013310 (2015).
[25] C.-C. Huang, G. Gompper, and R. G. Winkler, Phys. Rev. E **86**, 056711 (2012).
[26] S. H. Lee and R. Kapral, J. Chem. Phys. **121**, 11163 (2004).
[27] J. T. Padding, A. Wysocki, H. Löwen, and A. A. Louis, J. Phys.: Condens. Matter **17**, S3393 (2005).
[28] I. O. Götze and G. Gompper, Phys. Rev. E **82**, 041921 (2010).
[29] J. K. Whitmer and E. Luijten, J. Phys.: Condens. Matter **22**, 104106 (2010).
[30] M. Belushkin, R. G. Winkler, and G. Foffi, J. Phys. Chem. B. **115**, 14263 (2011).
[31] S. Poblete, A. Wysocki, G. Gompper, and R. G. Winkler, Phys. Rev. E **90**, 033314 (2014).

[32] C. C. Huang, G. Gompper, and R. G. Winkler, J. Chem. Phys. **138**, 144902 (2013).
[33] M. Theers and R. G. Winkler, Phys. Rev. E **91**, 033309 (2015).
[34] J. P. Hansen and I. R. McDonald, *Theory of Simple Liquids* (Elsevier, New York, 1990).
[35] J. W. Dufty, Phys. Rev. A **30**, 1465 (1984).
[36] M. Ernst, E. Hauge, and J. Van Leeuwen, Phys. Rev. A **4**, 2055 (1971).
[37] T. Ihle and D. M. Kroll, Phys. Rev. E **63**, 020201(R) (2001).
[38] C.-C. Huang, A. Chatterji, G. Sutmann, G. Gompper, and R. G. Winkler, J. Comput. Phys. **229**, 168 (2010).
[39] A. W. Lees and S. F. Edwards, J. Phys. C **5**, 1921 (1972).
[40] M. P. Allen and D. J. Tildesley, *Computer Simulation of Liquids* (Oxford University Press, Oxford, 1989).
[41] R. G. Winkler, in *Hierarchical Methods for Dynamics in Complex Molecular Systems*, edited by J. Grotendorst, G. Sutmann, G. Gompper, and D. Marx (Forschungszentrum Jülich GmbH, Jülich, 2012), Vol. 10 of IAS Series.
[42] M. Ripoll, K. Mussawisade, R. G. Winkler, and G. Gompper, Europhys. Lett. **68**, 106 (2004).
[43] V. Kumaran, Phys. Rev. Lett. **96**, 258002 (2006).